Journal of Alloys and Compounds 960 (2023) 170614

Contents lists available at ScienceDirect

Journal of Alloys and Compounds

journal homepage: www.elsevier.com/locate/jalcom

Research Article

Development and optimization of novel sulfur-containing Ti-based bulk metallic glasses and the correlation between primarily crystallizing phases, thermal stability and mechanical properties

Lucas M. Ruschel [a,*], Bastian Adam [a], Oliver Gross [b], Nico Neuber [a], Maximilian Frey [a], Hans-Jürgen Wachter [c], Ralf Busch [a]

[a] Chair of Metallic Materials, Saarland University, 66123 Saarbrücken, Germany
[b] Amorphous Metal Solutions GmbH, 66424 Homburg, Germany
[c] Heraeus AMLOY Technologies GmbH, 63450 Hanau, Germany

ARTICLE INFO

Article history:
Received 6 December 2022
Received in revised form 20 April 2023
Accepted 16 May 2023
Available online 18 May 2023

Keywords:
Bulk metallic glass
Titanium alloys
Biomaterials
Mechanical properties
Thermal stability
Sulfur

ABSTRACT

The effect of sulfur on the glass forming ability, thermal stability and mechanical properties of the eutectic alloy $Ti_{33.4}Zr_{33.3}Cu_{33.3}$ was investigated by conventional X-ray diffraction, differential scanning calorimetry and 3-point flexural experiments. A novel region of bulk glass formation with a critical casting diameter of up to 4 mm was found in the quaternary Ti-Zr-Cu-S system, however, brittle fracture behavior was predominant. Various alloying strategies were employed to improve mechanical properties and a compositional transition from brittle to ductile fracture has been identified (e.g. for $Ti_{36}Zr_{33.5}Cu_{24.5}S_6$). A change of the primary precipitating phases from a C14 Laves to an intermetallic $(Ti,Zr)_2Cu$ phase can be observed, as well as a stabilization of the supercooled liquid. The origin of the thermally unstable behavior in Ti-based bulk metallic glasses is traced back to the easy formation of the icosahedral phase upon heating, which is structurally close to the supposedly predominant icosahedral short-range order in the amorphous state. The systematic study carried out in this work indicates a strong correlation between primary crystallizing phase and thermal stability, both pointing to the frozen short-range order in the amorphous state which is predetermining the mechanical properties. The transition from the Laves to the intermetallic $(Ti,Zr)_2Cu$ phase as well as the enlarged supercooled liquid region appear to be directly related to a destabilization of the icosahedral short-range order and ultimately to the improved mechanical properties.

1. Introduction

Metallic glasses have been subject of intense research since their discovery in the early 1960s [1]. Unlike crystalline materials, atoms in amorphous metals are arranged randomly on a long-range order but exhibit a distinct short- and medium range order on atomic length scales. Compared to crystalline metals of similar composition, they are characterized by significantly higher strength, exceedingly high hardness and outstanding elastic properties [2]. Due to the high cooling rates required to suppress crystallization and enable glass formation, it is particularly challenging to produce amorphous metals even in the order of a few millimeters. Alloy systems that exceed the critical casting thickness of 1 mm in conventional casting processes are called bulk metallic glasses (BMGs). These include, for instance, Zr- [3], Ti- [4], Pd [5], Pt- [6,7], Au-[8], Mg-[9]. Fe- [10], and Ni- [11,12] based systems. Among these metal-based BMGs, Ti-based BMGs possess great potential for promising applications due to their low density, high strength and consequently high specific strength [13–15]. The critical problem of known Ti-based alloys with exceptionally good glass-forming ability (GFA) combined with low density is the presence of the toxic element Be, preventing their use in medical applications [15,16]. Other good glass formers without Be include the element Pd, an undesirable element for a lightweight material due to its high density and cost [16,17]. Recently, a promising alternative has been discovered by our group with the new family of S-containing alloys, showing high glass-forming ability without the use of the mentioned undesired elements. Based on various eutectic alloys, different bulk glass forming compositions have been derived in the S bearing Ti-based system. Starting from the ternary eutectic $Ti_{65.5}Ni_{22.5}Cu_{12}$ [18], BMGs with good GFA and high Ti content were developed using small amounts of 4 at% S [19]. In Ref. [20], originating from the binary Ti-Ni and Ti-Cu eutectics,

* Corresponding author.
E-mail address: lucas.ruschel@uni-saarland.de (L.M. Ruschel).

https://doi.org/10.1016/j.jallcom.2023.170614

bulk glass formation up to 3 mm with additions of Zr, Cu, Ni and a S content of 8 at% were achieved. Among them, the Ni-free Ti-Zr-Cu-S alloys (e.g. $Ti_{40}Zr_{35}Cu_{17}S_8$) are of particular interest for biomedical applications, as few to no metal ions are released into solution due to their excellent electrochemical corrosion resistance [17,20]. Sulfur itself is considered uncritical, as it belongs to the minerals and is an important component of several amino acids of the human organism [21]. This ensures little to no interaction with human cells and therefore classifies them as biocompatible. In particular, crystalline Ti alloys are widely used in orthopedic prosthetics and dental implants due to their high corrosion resistance and good biocompatibility [22–25]. However, their main drawback is the high elastic modulus compared to that of a human bone causing effects like stress shielding and loosening of the implants [22], whereas the unique structure of amorphous Ti-based BMGs with a relatively low elastic modulus in combination with high engineering yield strength enables them to emerge as a promising alternative to conventional crystalline implants [23].

As origin of the present work, the ternary eutectic $Ti_{33.4}Zr_{33.3}Cu_{33.3}$ (E5) on the copper-rich side was chosen as new starting point for alloy development. Arroyave et al. reported this eutectic E5 as the point with the lowest liquidus temperature in the Ti-Zr-Cu system, an ideal starting point, as the liquid state is stabilized to very low temperatures, promoting glass formation [26,27]. Molokanov and Chebotnikov studied a wide range of alloys in the quaternary Ti-Zr-Ni-Cu system, including the $Ti_{66.7-x}Zr_xCu_{33.3}$ ternary alloy series with a maximum critical casting thickness of amorphous ribbons of 250 µm for $Ti_{26.7}Zr_{40}Cu_{33.3}$ [28]. The critical thickness of the eutectic composition E5 is reported as ~200 µm [28]. Many systems have shown that minor additions of another element result in metallic glasses with improved properties and enhanced GFA, if the proper minor alloying element is chosen for the respective base alloy [29–31]. In Ti-based systems, S has already been proven to be very beneficial for amorphization by increasing the topological variability and complexity of the system, hence following the empirical rules for glass formation [19,20,27,32]. Recently, Wilden et al. have shown that S reduces the melt dynamics in Ti-based glass-forming systems, presumably caused by the formation of covalent interactions [33]. Apart from metalloid elements (e.g. S, Si or B), metals such as Sc, Ni or Al are frequently used as minor additions [25,34–37]. The latter is of particular interest as it is a light element that further reduces the density of the system, promoting lightweight applications. With respect to alloys not directly associated for medical applications, Ni, which is topologically equivalent to Cu, can contribute to enhanced glass formation [20,36,38].

In our previous study, it was found that Ni-free Ti-based bulk metallic glasses can be formed in the Ti-Zr-Cu-S alloy system, but the GFA was limited up to only 3 mm [20]. This work focuses primarily on different alloying strategies in the Ti-Zr-Cu-S system and its effects on GFA, thermal stability and mechanical properties. The primary goal was to enable a larger application field by enhancing the GFA, however, it was found that the mechanical properties (ductile or brittle fracture behavior) are remarkably sensitive to small compositional changes. The mechanism causing this distinctive change in the mechanical performance is found to be related to the liquid and glassy structure, which are known to be dominated by an icosahedral short-range order (ISRO) in Ti-based alloys [39–41]. To deepen the understanding of the embrittlement mechanism in the studied alloys and eventually in Ti-based BMGs in general, the results are further supported by systematic studies of Ni and Al additions, causing similar changes in fracture behavior. Ultimately, this allows the development of Ti-based metallic glasses with improved GFA as well as desired mechanical properties to enable their use in potential biomedical applications.

2. Experimental procedure

2.1. Sample production

The alloys were prepared from high purity raw elements: Ti (99.995 wt%), Zr (99.99 wt%), Cu (99.999 wt%), Ni (99.99 wt%), S (99.9995 wt%) and Al (99.99 wt%). To add S into the composition, a custom-made Cu-S pre-alloy was used, synthesized from high purity Cu and S in a quartz tube under high purity argon atmosphere with the composition $Cu_{67}S_{33}$ (at%). Subsequently, the mass of the pre-alloy was checked to identify any mass loss compared to the weighted-in elements. The conservation of mass allows an accurate determination of the final Cu-S composition assuming that only S (low boiling point) and no Cu is lost in the process. A detailed description of the production process is given in Ref. [42]. Subsequently, the raw elements were alloyed together with the pre-alloy in an electric arc furnace under a Ti-gettered argon atmosphere. To ensure homogeneous distribution of the elements, the ingots were flipped and remelted at least 5 times. Afterwards, the samples were cast under a Ti-gettered high purity argon atmosphere into water cooled copper molds using a custom-built suction casting machine. For the poorer glass formers, plate-shaped specimens with thicknesses of less than 1 mm were cast. Otherwise, rod-shaped samples with different diameters (≥ 2 mm) were fabricated to determine the critical casting diameter.

2.2. X-ray diffraction and calorimetric analysis

The samples used for X-ray diffraction (XRD) and differential scanning calorimetry (DSC) were cut from the cylindrical rods at a height of 10 mm from the bottom right next to each other. To verify the amorphous structure as well as identify the crystalline phases, XRD measurements were conducted using a PANalytical X'Pert Pro diffractometer and a D8-A25-Advance diffractometer with monochromatic Cu-Kα radiation. The cross section of all specimens, including the beams for the mechanical tests, were characterized to obtain information from the inner region of the sample, most critical for crystal formation as it is experiencing the lowest cooling rate. Thermal analyses were performed at heating rates of 1 K/s in Cu pans under a constant high-purity argon flow using a power-compensated Perkin Elmer DSC 8000 to determine the onset of the glass transition temperature, T_g, and the onset of the primary crystallization, T_x, of the amorphous samples.

2.3. Mechanical testing

Metallic materials are conventionally tested in tensile tests. However, even metallic glasses that are microscopically (intrinsically) ductile behave macroscopically brittle in this mode due to the formation of one shear band under approximately 45° to the tensile axis. This single shear band propagates and leads to catastrophic failure. For this reason, the mechanical parameters such as Young's modulus, yield strength, fracture strength and total strain were determined in a 3-point beam bending (3PBB) setup using a Shimadzu universal testing machine, as it allows the formation of multiple shear banding ultimately enabling the observation of intrinsic ductility. All beam-shaped specimens feature a rectangular cross-section and were cast in the dimension of 3 mm × 2 mm x 25 mm using the copper mold suction casting technique and subsequently sanded with up to 1200 grit SiC paper. The support span L was 20 mm. Both, the applied force F and the deflection D at the center of the beam were recorded during the test. The engineering stress σ at the sample surface and the strain ε at the midpoint of the beam were calculated by simple beam mechanics theory using the equations:

$$\sigma = \frac{3FL}{2wh^2} \quad (1)$$

and

$$\varepsilon = \frac{6Dh}{L^2} \quad (2)$$

with the height h and the width w of the beam.

The deflection rate $\dot{D}$, i.e. the velocity of the crosshead, was constant at 0.3 mm/min. For beam specimens with thicknesses about 2 mm and a support length of 20 mm, Eq. 2 provides a strain rate of 1.5×10^{-4} s^{-1} at the outer fiber if $\dot{D}$ is used instead of D.

To determine a meaning strain, the ramp-up behavior at the beginning of the stress-strain curve was corrected, as described in Fig. SI1 of the supplementary information. Optimized casting parameters allow defects such as micropores to be largely eliminated. However, to exclude random scattering of the results in case of such defects, three test specimens were tested for each composition.

3. Results

3.1. Alloy development

The GFA and thermal stability of the novel Ti-based alloys were investigated by XRD and thermal analysis upon heating from the glassy state at a rate of 1 K/s. Both properties are fundamental for the production and processing of BMGs. Fig. 1a and b summarize the XRD results of the S addition series $(Ti_{33.4}Zr_{33.3}Cu_{33.3})_{100-x}S_x$ (x=0, 2, 4, 6, 8, 10, hereafter E5-S_x) for various thicknesses, allowing to determine the critical casting thickness of the studied alloys. For dimensions below 1 mm, plate-shaped samples were tested instead of rod-shaped samples. The critical casting thickness of the compositions containing 2–10 at% S reveal no sharp Bragg peaks from any crystalline phase, but the typical diffusive diffraction maxima representative of monolithic metallic glasses. However, the alloy without S cannot be produced as a glass in a conventional copper mold casting process due its low GFA, e.g. small critical casting thickness, d_c, of d_c ~200 µm [28]. The compositions that turned out amorphous were then cast into molds one millimeter larger than the critical casting thickness (d_c+1 mm) to determine the primary crystalline phases, as shown in Fig. 1b. Two dominating crystalline phases, the C14 Laves phase (Frank-Kasper structure) and intermetallic $(Ti,Zr)_2Cu$ (tetragonal structure) can be identified by XRD. In equilibrium conditions a bcc phase is additionally reported by Arroyave et al. for the ternary eutectic [26]. To conclude, an appropriate addition of S up to 4 at% significantly enhances the GFA in the Ti-Zr-Cu system, leading to a d_c of up to 4 mm. Further additions above 4 at % lead to a continuous decrease of the GFA to a d_c of 3, 0.75 and 0.5 mm for E5-S_6, E5-S_8 and E5-S_{10}, respectively.

The corresponding DSC scans of fully amorphous samples with increasing S-content are given in Fig. 1c, except for E5-S_0, as no amorphous specimen could be produced in conventional copper mold casting due to the limited GFA. The crystallization proceeds via multiple exothermic crystallization reactions for all compositions, although not all of them feature a distinct endothermic event associated with the glass transition. For instance, no distinct glass transition could be observed for E5-S_2, as the alloy starts to crystallize immediately as the atomic mobility is regained in the vicinity of the glass transition. Towards E5-S_{10}, the signal of the glass transition event is getting more and more pronounced, as the onset of crystallization is shifted continuously to higher temperatures, reflecting a stabilization of the supercooled liquid region (SCLR), as summarized in Table 1. The onset temperature of the glass transition T_g for those showing one as well as the onset of crystallization T_x is marked with arrows in each curve. Each alloy was also heat treated until the first crystallization was completed and subsequently cooled

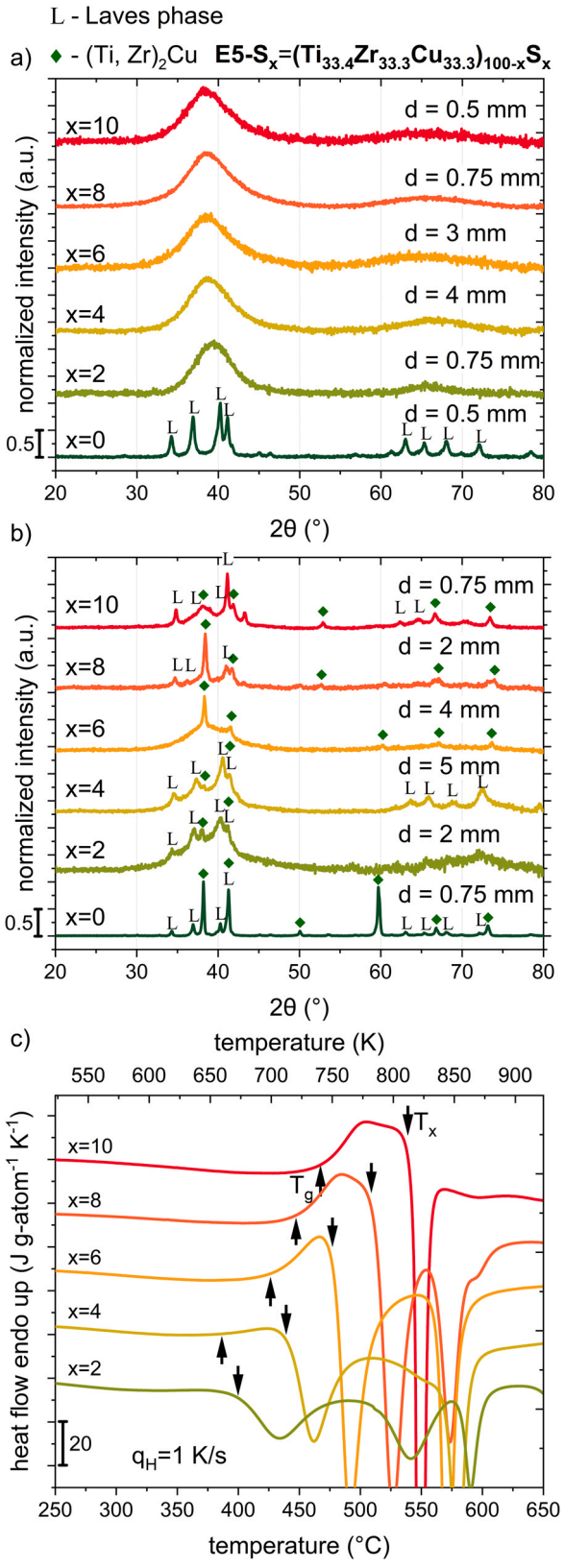

Fig. 1. XRD patterns of $(Ti_{33.4}Zr_{33.3}Cu_{33.3})_{100-x}S_x$ (x=0, 2, 4, 6, 8, 10) at different thicknesses with (a) showing the critical casting thickness of as-cast samples, despite the one without S that could not be produced amorphously and (b) partially crystallized samples closely above the critical casting thickness. (c) DSC Scans measured with a heating rate of 1 K/s for all amorphous compositions.

Table 1
Calorimetric properties of fully amorphous samples studied in this work. T_g represents the onset of the glass transition temperature, T_x determines the onset of the primary crystallization, and ΔT_x determines the width of the SCLR (ΔT_x=T_x-T_g). The critical diameter d_c corresponds to XRD amorphous samples produced by copper mold casting.

Composition (at%)	T_g (K)	T_x (K)	ΔT_x (K)	d_c (mm)
$Ti_{33.4}Zr_{33.3}Cu_{33.3}$ (E5-S_0)	-	-	-	~ 0.2 [28]
$(Ti_{33.4}Zr_{33.3}Cu_{33.3})_{98}S_2$ (E5-S_2)	-	673	-	0.75
$(Ti_{33.4}Zr_{33.3}Cu_{33.3})_{96}S_4$ (E5-S_4)	660	712	52	4*
$(Ti_{33.4}Zr_{33.3}Cu_{33.3})_{94}S_6$ (E5-S_6)	699	751	52	3
$(Ti_{33.4}Zr_{33.3}Cu_{33.3})_{92}S_8$ (E5-S_8)	721	782	61	0.75
$(Ti_{33.4}Zr_{33.3}Cu_{33.3})_{90}S_{10}$ (E5-S_{10})	740	812	72	0.5
$Ti_{34}Zr_{32.8}Cu_{28.2}S_5$ (CL-S_5)	663	717	54	4*
$Ti_{36}Zr_{33.5}Cu_{24.5}S_6$ (CL-S_6)	668	723	55	4
$Ti_{38}Zr_{34.3}Cu_{20.7}S_7$ (CL-S_7)	675	729	54	4
$Ti_{40}Zr_{35}Cu_{17}S_8$ (CL-S_8)	677	730	53	3 [20]
$Ti_{36}Zr_{33.5}Cu_{22.5}Ni_2S_6$	666	713	47	4
$Ti_{36}Zr_{33.5}Cu_{20.5}Ni_4S_6$	663	709	46	4
$Ti_{36}Zr_{33.5}Cu_{18.5}Ni_6S_6$	-	704	-	~3**
$Ti_{36}Zr_{33.5}Cu_{16.5}Ni_8S_6$	-	706	-	~3**
$Ti_{36}Zr_{33.5}Cu_{14.5}Ni_{10}S_6$	-	711	-	~3**
$Ti_{36}Zr_{33.5}Cu_{12.5}Ni_{12}S_6$	-	706	-	~3**
$(Ti_{36}Zr_{33.5}Cu_{24.5}S_6)_{99}Al_1$	670	720	50	4
$(Ti_{36}Zr_{33.5}Cu_{24.5}S_6)_{98}Al_2$	676	726	50	4*
$(Ti_{36}Zr_{33.5}Cu_{24.5}S_6)_{97}Al_3$	677	727	50	4
$(Ti_{36}Zr_{33.5}Cu_{24.5}S_6)_{96}Al_4$	680	729	49	4
$(Ti_{36}Zr_{33.5}Cu_{24.5}S_6)_{95}Al_5$	695	736	41	4

* Highest GFA of the respective series
** 2 mm × 3 mm amorphous beams

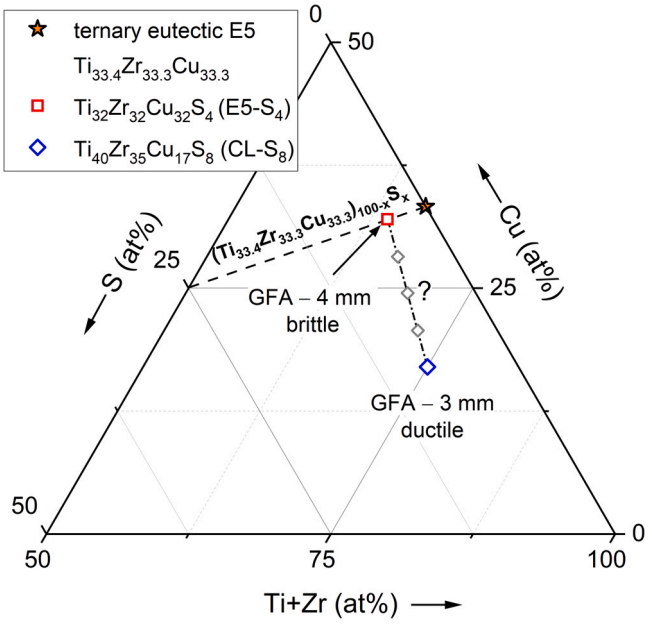

Fig. 2. Quasi-ternary (Ti,Zr)-Cu-S diagram with the best-found glass formers $Ti_{32}Zr_{32}Cu_{32}S_4$ of this work as well as $Ti_{40}Zr_{35}Cu_{17}S_8$ from Ref. [20]. The grey squares indicate the "connection line" compositions.

down to determine the first crystalline phase ex-situ by XRD (see Fig. SI2). The analysis reveals that the primary phase upon heating changes from an icosahedral phase (I-phase) for E5-S_x (x=2,4,6,8) to the Laves phase for E5-S_{10}. Therefore, the observability of the glass transition through the increasing stabilization of the SCLR to 72 K for E5-S_{10} is directly connected to the destabilization of the quasi-crystalline I-phase. However, the maximum in GFA and SCLR does not coincide with each other and show contrary behavior. Among the alloys studied, the supercooled liquid of the best glass former E5-S_4 behaves thermally very unstable with almost no SCLR, in contrast to the most stable composition E5-S_{10} which shows a poor GFA.

As will be shown later, the best alloy E5-S_4 with respect to GFA is mechanically brittle, whereas the amorphous alloy $Ti_{40}Zr_{35}Cu_{17}S_8$ developed by Kuball et al. in the same quasi-ternary Ti-Zr-Cu-S system behaves ductile in 3-point flexural tests [20]. The objective of further alloy optimization is to scan the compositional space in between to observe and understand the transition from brittle to ductile fracture behavior. The region of interest is depicted in the quasi-ternary (Ti,Zr)-Cu-S diagram in Fig. 2 and is called “connection line” in the following. The specimens are labeled “CL” accordingly. These include the compositions $Ti_{32}Zr_{32}Cu_{32}S_4$, $Ti_{34}Zr_{32.8}Cu_{28.2}S_5$, $Ti_{36}Zr_{33.5}Cu_{24.5}S_6$, $Ti_{38}Zr_{34.3}Cu_{20.7}S_7$ and $Ti_{40}Zr_{35}Cu_{17}S_8$, which are further referred to as E5-S_4 (as before), CL-S_5, CL-S_6, CL-S_7 and CL-S_8, respectively. The composition E5-S_4 (red square) results from the alloy development shown in Fig. 1, while CL-S_8 (blue square) is the best glass forming alloy described in Ref. [20]. The intervening alloys CL-S_5 to CL-S_7 (grey squares) are calculated according to a linear equation. More details on the determination are provided in the supplementary information.

The XRD results of the “connection line” of both bulk glass forming regions are shown in Fig. 3a and b for the casting thicknesses of 4 mm and 5 mm, respectively. The best composition in terms of critical casting thickness from the S series E5-S_4 is plotted again to illustrate the trend in GFA and the change in the primary precipitating phases. Referring to Fig. 3a, a wide GFA range of 4 mm was found ranging from E5-S_4 to CL-S_6. CL-S_7 also exhibits a mostly amorphous XRD pattern but shows first signs of primary crystallization at the main peak of the amorphous halo. The primary precipitating phase $(Ti,Zr)_2Cu$ is more prominent in CL-S_8, which exhibits a GFA of 3 mm according to Ref. [20], hence is not expected to solidify without crystallization at 4 mm. The change of the primary crystalline phases in cooling from the equilibrium melt can be identified more precisely in Fig. 3b, where the Laves phase in E5-S_4 changes to a coexistence of the Laves and intermetallic $(Ti,Zr)_2Cu$ phase in CL-S_5, followed by quasi-binary $(Ti,Zr)_2Cu$ in CL-S_6 to CL-S_8. The alloy with the highest GFA, CL-S_5, exhibits a mostly amorphous pattern in addition to a few Bragg peaks, condensing to a critical casting thickness slightly below 5 mm. Interestingly, the maximum in GFA is exactly located where the primary crystalline phases are changing. By moving compositionally closer to CL-S_8, the GFA drops continuously due to the primary formation of the less complex intermetallic $(Ti,Zr)_2Cu$. The corresponding DSC measurements with an increasingly thermal stability towards CL-S_8 is shown in Fig. 3c with the thermal properties summarized in Table 1. All further alloy development strategies were subsequently performed on CL-S_6 ($Ti_{36}Zr_{33.5}Cu_{24.5}S_6$) rather than the best composition in terms of GFA, CL-S_5, as it exhibits superior mechanical properties and no brittle fracture failure, as will be shown later (Fig. 5).

Fig. 4a and b show the XRD data of 4 mm and 5 mm rods of $Ti_{36}Zr_{33.5}Cu_{24.5-y}Ni_yS_6$ (y=2, 4, 6, 8, 10, 12) where Cu is continuously substituted with Ni. Regarding a structural point of view, Ni and Cu are considered topologically equivalent due to their similar atomic size [43]. Therefore, both are frequently considered interchangeable [44]. Low Ni contents do not lead to any noticeable change in the GFA compared to the Ni free variant, as both alloys (y=2 and y=4) still completely vitrify in 4 mm rods and show crystallization for a diameter of 5 mm. However, higher Ni contents lead to a continuous decline in GFA due to the formation of the I-phase, followed by the C14 Laves phase. A similar transition from an amorphous structure to the formation of quasicrystals and Laves phase was also reported in another S-bearing BMG system based on the ternary Ti-Ni-Cu eutectic [19]. In general, both crystalline phases are common and frequently reported in Ti-based BMGs [15,19,36,41,45–47]. Next to Ni addition, the influence of Al as light element was investigated by equiatomic substitution, keeping the elemental ratios of the mechanically best composition CL-S_6 constant as shown in Fig. 4c and d.

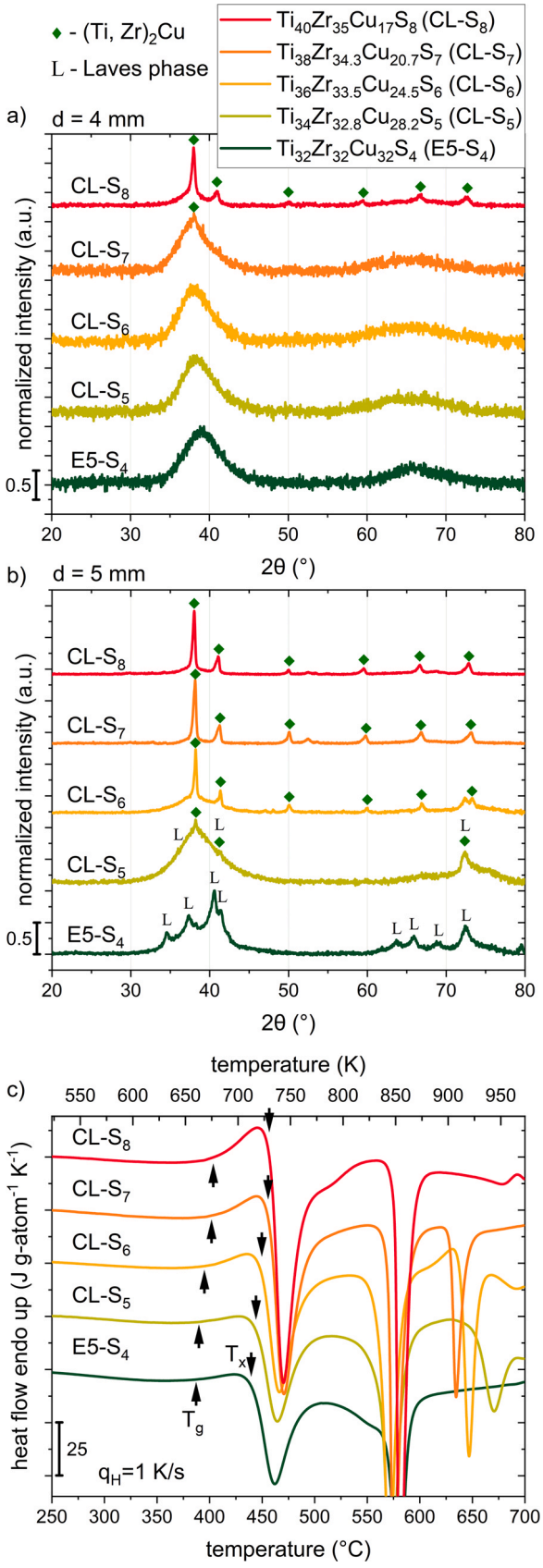

Fig. 3. (a) and (b) shows the X-ray diffraction patterns of 4 mm and 5 mm as-cast samples of the "connection line" compositions. (c) The corresponding DSC scans were acquired on fully amorphous samples at a rate of 1 K/s.

Aluminum was considered rather as microalloying element and was added in small amounts, up to a maximum of 5 at% Al. All Al-containing compositions solidify glassy in 4 mm molds, indicating no deterioration in GFA. In case of 5 mm casts, Al addition of just 1 at% is not sufficient to improve the GFA, yielding a similar critical casting thickness as the "base" alloy CL-S_6 (compare z=1 of Fig. 4d to CL-S6 of Fig. 3b). Further Al alloying of about 2–3 at% result in the biggest improvement with a XRD pattern indicating a mostly glassy sample superimposed by a few $(Ti,Zr)_2Cu$/Laves Bragg peaks. The declining GFA with increasing Al content goes again hand in hand with a change of the primary crystallizing phase from the $(Ti,Zr)_2Cu$ intermetallic to a C14 Laves phase. Unlike the Ni series, the phase change does not occur through the intermediate step of the icosahedral phase formation. This effect of improved GFA at minor addition of elements with further deterioration at larger amounts is often observed in literature for the so-called micro-alloying technique [30]. Fig. 4e and f depict the corresponding DSC scans, with the Ni series showing a continuous destabilization of the glass transition until no T_g is observable (Ni ≥ 6 at%), and the Al series showing only a slight reduction of the SCLR. The characteristic temperatures are summarized in Table 1.

3.2. Mechanical properties

Monitoring the mechanical properties and their evolution is particularly important for the development of application-oriented alloys, especially as S-containing Ti-based BMGs allow the usage of industrial-grade raw material without significant deterioration of GFA, as shown by Kuball et al. for $Ti_{40}Zr_{35}Cu_{17}S_8$ in Ref. [20]. A certain amount of ductility is of particular interest to prevent sudden failure in case the applied load unexpectedly exceeds the yield strength. Prior to testing, the amorphous structure of the flexural beams was verified by XRD. Fig. 5a, b, and c show the 3PBB engineering stress-strain curves for three alloy series developed in this work, the "connecting line", the Ni series as well as the Al series. The novel glass forming alloy E5-S_4 based on the Ti-Zr-Cu eutectic E5 with a GFA of 4 mm fails brittle in 3PBB experiments with a total strain below 2%. Such premature failure is likely related to a low fracture toughness, resulting in poor resistance to defects such as micropores or surface scratches. These allow crack propagation more easily in the tensile loaded region of the beams, turning 3PBB experiments into an elaborate way to study the intrinsic mechanical properties. Moving compositionally towards $Ti_{40}Zr_{35}Cu_{17}S_8$, the transition from brittle to ductile fracture behavior occurs exactly at the intermediate alloy composition $Ti_{36}Zr_{33.5}Cu_{24.5}S_6$ (CL-S_6). This composition also features the largest total strain to failure of around 4.2% in bending of the studied alloys. Therefore, it was chosen as new origin for alloy development of the Ni and Al series, although it was not the composition with the highest GFA. The stepwise Ni addition shown in Fig. 5b led to a decrease in ductility, followed by complete embrittlement at Ni contents above 2 at%. Despite their amorphous structure, the latter do not even reach their yield strength. Similar, but less catastrophic embrittlement is also observed throughout the Al series in Fig. 5c. However, the best composition $(Ti_{36}Zr_{33.5}Cu_{24.5}S_6)_{98}Al_2$ in terms of GFA still reaches its yield strength and exhibits minor ductility before fatal fracture occurs. Al contents above 2 at% ultimately led to premature, brittle failure. The Young's moduli of all different compositions studied in this work range from 83 to 89 GPa in bending. A detailed summary of the mechanical properties σ_{yield} (0.2%), $\sigma_{fracture}$, $E_{bending}$ and ε_{total} corresponding to the yield strength at 0.2% strain, the fracture strength, the Young's modulus in bending and the maximum achieved strain, respectively, is provided in Table 2.

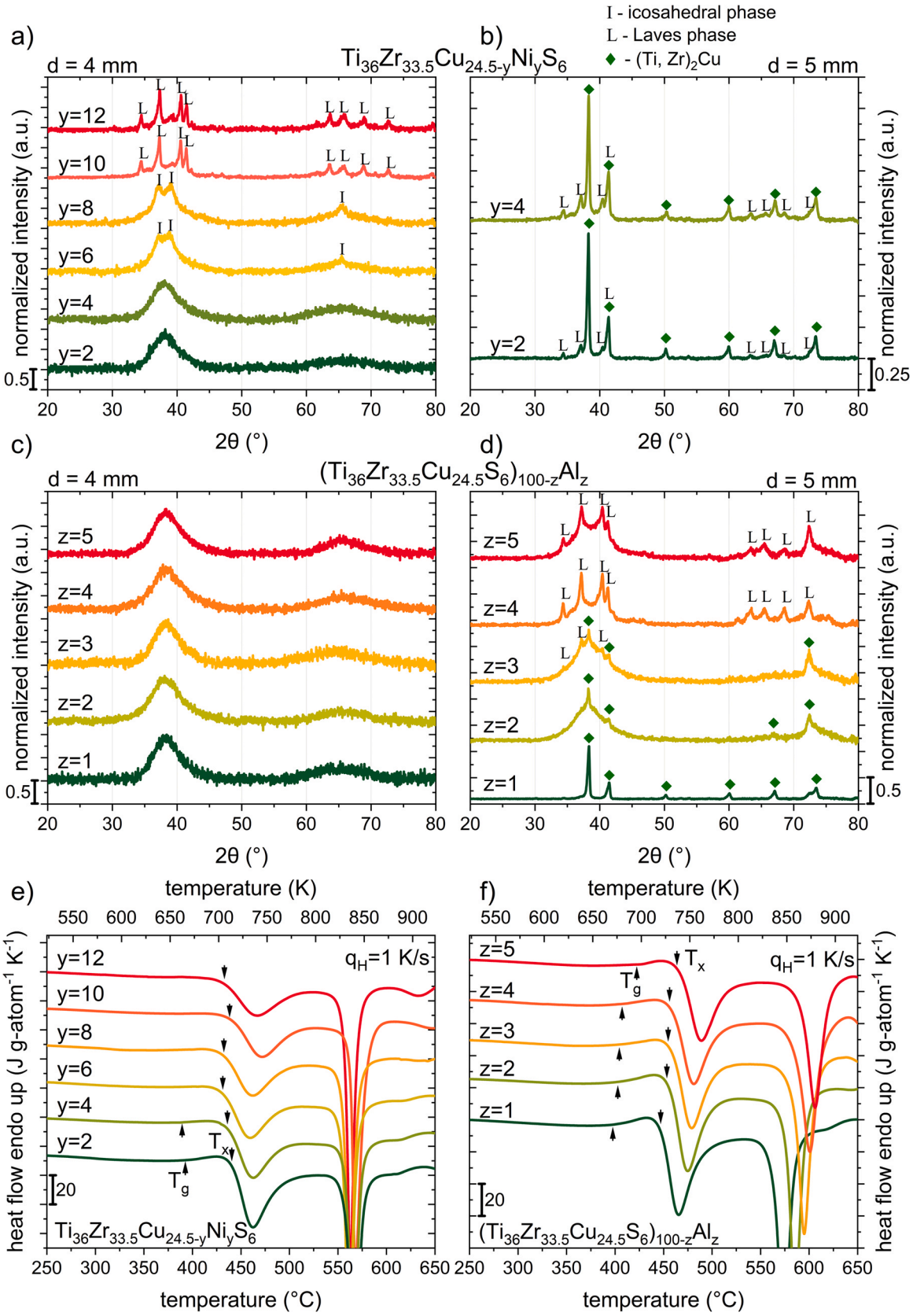

Fig. 4. XRD patterns of 4 mm and 5 mm rods for the evaluation of the critical casting thickness of the Ni series $Ti_{36}Zr_{33.5}Cu_{24.5-y}Ni_yS_6$ (y=2, 4, 6, 8, 10, 12) in (a) and (b) and for the Al series $(Ti_{36}Zr_{33.5}Cu_{24.5}S_6)_{100-z}Al_z$ (z=1, 2, 3, 4, 5) in (c) and (d). (e) and (f) depicts the corresponding DSC scans of both series acquired at a rate of 1 K/s.

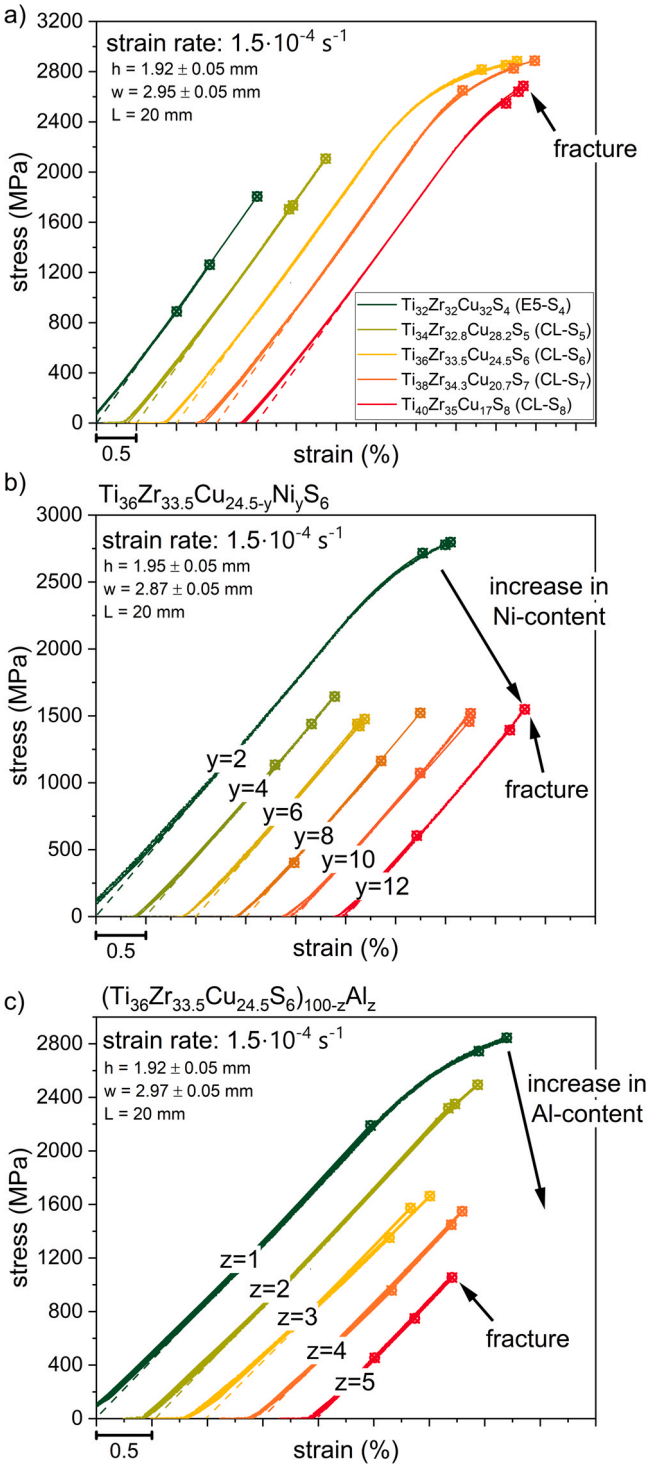

Fig. 5. Engineering stress-strain curves of different bulk glass forming alloy compositions measured in a 3PBB setup. A total strain of less than 2% indicates a brittle fracture behavior.

4. Discussion

The XRD analyses of the investigated quaternary Ti-Zr-Cu-S as well as quintenary Ti-Zr-Cu-S-Al alloys reveal the C14 Laves phase as well as the intermetallic compound $(Ti,Zr)_2Cu$ to be the primary crystallizing phases. Considering the composition of the respective alloy, the latter results from continuous solubility of Ti and Zr in the tetragonal $(Ti,Zr)_2Cu$ phase throughout the ternary phase diagram from Ti_2Cu to Zr_2Cu [26]. The mixture of Ti and Zr atoms in the tetragonal sub-lattices leads to changes in the lattice parameters (Vegard's law), resulting in a shift of the Bragg peaks as exemplarily shown for CL-S_6 in Fig. SI3 in the supplementary information. A similar change in the primary crystals is observed upon Ni addition to the quaternary Ti-Zr-Cu-S system, although an additional quasicrystalline I-phase is formed as intermediate step. A stabilization of the I-phase by Ni has been observed several times, for example in the Ti-Ni-S [20] and Ti-Zr-Ni-Cu [48] system. Since Cu and Ni are considered to be topologically equivalent, the substitution of both elements should not affect the structure, yet Stiehler et al. found significant structural differences in the short- and medium-range order of Zr-based alloys, which were mainly attributed to diversified local electronic interactions [49]. In combination with the strong negative enthalpy of mixing of Ni with Ti and Zr (ΔH_{mix}^{Ti-Ni}=−35 kJ/mol, ΔH_{mix}^{Zr-Ni}=−49 kJ/mol [44]), an icosahedral structure seems to be promoted in the liquid state, which is supported by high-energy X-ray diffraction experiments of Goldman et al., who observed a progressive increase of an ISRO by the addition of Ni to binary Ti-Zr [40]. Saida et al. also found that elements having a positive or weak chemical affinity to one of the constitutional elements (ΔH_{mix}^{Cu-Ni}=4 kJ/mol [44]) in Zr- or Hf-based glass-forming systems are beneficial for the precipitation of the I-phase [50]. Moreover, the I-phase commonly forms as primary phase upon heating from the glassy state, causing the thermally unstable behavior in most of the alloys studied and in general in Ti-based BMGs [15,45,51,52]. Some of them, mainly the Ni series, do not even show a pronounced glass transition, as T_g is superimposed by primary crystallization. This thermal instability is expected to be related to structural similarities between the predominant ISRO in the liquid/amorphous state and the quasicrystalline I-phase, as frequently reported for Ti-based BMGs [19,39–41,53]. Those structural similarities result in a reduced interfacial energy and consequently, according to classical nucleation theory, in a reduced nucleation barrier for the I-phase [41,54–57]. The importance of the interfacial energy for the GFA of metallic glasses has been shown for Pt-P-based liquids [58]. In these liquids, a high interfacial energy is able compensate a high driving force for crystallization and a fragile liquid behavior. In the case of the Ti-based glasses, a low interfacial energy due to a pronounced ISRO results in an immediate crystallization as soon as atomic mobility is restored in the vicinity of the glass transition. Similar phenomena were also observed in Al-based BMGs with high Al-contents, where the glass transition is superimposed by the rapid formation of fcc α-Al nanocrystals [59–61]. Another indication for a predominant ISRO is reflected in a change of the primary phase upon cooling from the tetragonal $(Ti, Zr)_2Cu$ to an icosahedral or Laves phase, as the latter contains a high proportion of icosahedral clusters [40,62,63]. This means that elements stabilizing an ISRO in Ti-based BMGs result in reduced thermal stability.

Our study suggests that the addition of S is an effective way to retard/suppress the formation of the I-phase during heating, as demonstrated for the E5-S_x series with increasing S content. Ultimately S addition leads to a distinct glass transition and stable SCLR (Fig. 1c) prior to the emergence of crystallization. The positive influence of S on thermal stability seems to be an almost universal feature, as it has already been demonstrated in various BMG systems, like Cu-, Zr-, Ni and Pd-based ones [32,42], [64]. Interestingly, the maximum GFA in the Ti-Zr-Cu-S system ($Ti_{32}Zr_{32}Cu_{32}S_4$) coincides with that reported in the Ti-Zr-Ni-Cu-S system ($Ti_{58}Zr_{7.5}Ni_{18.5}Cu_{12}S_4$) at a sulfur content of 4 at% [19]. Characteristic are the elements Ti and Zr as well as Cu and Ni, which each form a complete solid solution in their binary phase diagrams [65,66]. Furthermore, Ti and Zr have similar electron configurations, hence they can be considered chemically equivalent [67]. Ni and Cu, on the other hand, are often considered topologically equal

Table 2
Mechanical properties of the different alloy compositions investigated in this work: Engineering yield strength at 0.2% strain σ_{yield}, fracture strength $\sigma_{fracture}$, the Youngs modulus $E_{bending}$ and the total strain ε_{total} calculated from the flexural stress-strain curves.

Composition (at%)	σ_{yield} (GPa)	$\sigma_{fracture}$ (GPa)	$E_{bending}$ (GPa)	ε_{total} (%)
$Ti_{32}Zr_{32}Cu_{32}S_4$ (E5-S_4)	-	1.32 ± 0.4	87 ± 2	1.48 ± 0.4
$Ti_{34}Zr_{32.8}Cu_{28.2}S_5$ (CL-S_5)	-	1.85 ± 0.2	89 ± 1	2.09 ± 0.2
$Ti_{36}Zr_{33.5}Cu_{24.5}S_6$ (CL-S_6)	2.59 ± 0.1	2.85 ± 0.1	88 ± 1	4.23 ± 0.3
$Ti_{38}Zr_{34.3}Cu_{20.7}S_7$ (CL-S_7)	2.64 ± 0.1	2.79 ± 0.1	89 ± 1	3.59 ± 0.4
$Ti_{40}Zr_{35}Cu_{17}S_8$ (CL-S_8)	2.58 ± 0.1	2.63 ± 0.1	87 ± 1	3.25 ± 0.1
$Ti_{36}Zr_{33.5}Cu_{22.5}Ni_2S_6$	2.69 ± 0.1	2.76 ± 0.1	88 ± 1	3.44 ± 0.1
$Ti_{36}Zr_{33.5}Cu_{20.5}Ni_4S_6$	-	1.40 ± 0.2	88 ± 2	1.61 ± 0.2
$Ti_{36}Zr_{33.5}Cu_{18.5}Ni_6S_6$	-	1.45 ± 0.1	88 ± 1	1.66 ± 0.1
$Ti_{36}Zr_{33.5}Cu_{16.5}Ni_8S_6$	-	1.03 ± 0.5	85 ± 3	1.36 ± 0.3
$Ti_{36}Zr_{33.5}Cu_{14.5}Ni_{10}S_6$	-	1.35 ± 0.2	87 ± 2	1.59 ± 0.2
$Ti_{36}Zr_{33.5}Cu_{12.5}Ni_{12}S_6$	-	1.18 ± 0.4	88 ± 2	1.39 ± 0.5
$(Ti_{36}Zr_{33.5}Cu_{24.5}S_6)_{99}Al_1$	2.51 ± 0.2	2.59 ± 0.3	88 ± 1	3.54 ± 0.4
$(Ti_{36}Zr_{33.5}Cu_{24.5}S_6)_{98}Al_2$	-	2.39 ± 0.1	88 ± 1	2.77 ± 0.1
$(Ti_{36}Zr_{33.5}Cu_{24.5}S_6)_{97}Al_3$	-	1.53 ± 0.1	83 ± 2	1.82 ± 0.1
$(Ti_{36}Zr_{33.5}Cu_{24.5}S_6)_{96}Al_4$	-	1.32 ± 0.3	86 ± 2	1.55 ± 0.3
$(Ti_{36}Zr_{33.5}Cu_{24.5}S_6)_{95}Al_5$	-	0.65 ± 0.4	86 ± 3	0.86 ± 0.3

in metallic glass-forming systems due to their similar atomic radius [43]. Due to those similarities of Ti and Zr as well as Cu and Ni, the systems $Ti_{32}Zr_{32}Cu_{32}S_4$ and $Ti_{58}Zr_{7.5}Ni_{18.5}Cu_{12}S_4$ can be considered quasi-ternary (Ti,Zr)-(Cu,Ni)-S. From this point of view, the ratio of (Ti,Zr) to (Cu,Ni) is approximately equal in both systems with two to one, which seem to be crucial for the ideal sulfur content. The alloys studied by Kuball et al. support this working hypothesis, as they require a sulfur content of 8 at% for bulk glass formation (e.g. $Ti_{40}Zr_{35}Cu_{17}S_8$) due to a higher amount of Ti and Zr in the system [20]. Thus, the (Ti, Zr) to (Cu, Ni) ratio seems to define the optimal S-content, despite different properties (chemical and topological) are compared with each other. Fig. 6 shows the ideal S-content required to obtain the highest glass forming ability for different (Ti,Zr)/(Cu, Ni) ratios. The higher the Cu/Ni content, the less S is needed to obtain a maximum in the GFA, as shown for a Cu-based BMG $Cu_{46.3}Ti_{33.5}Zr_{10.8}Ni_{7.9}S_{1.5}$ (Vit101$S_{1.5}$) of the same system [68]. Furthermore, the maximum achievable S content (approx. 8.4 at%) for high (Ti,Zr) contents is marked in the diagram. Assuming that the GFA maximum follows the linear correlation, a simple Cu-S pre-alloy is no longer sufficient, and an additional Ti-S or Zr-S pre-alloy is necessary to achieve BMGs with (Ti,Zr) contents higher than ~75 at%. The optimal sulfur content as a function of the (Ti,Zr)/(Cu,Ni) ratio could be related to the size mismatch of the constituent atoms, which might exhibit an optimal dense random packing of the atoms at certain ratios. Lu et al. already pointed out that a defined atomic size distribution instead of an excessive size mismatch can lead to the highest packing density in the liquid and thus to an optimum in the GFA [69]. However, this does not explain why the optimum S content does not change significantly upon exchange of Ti and Zr, despite their significant atomic radius difference of around 10% [43]. In other words, the observed linear trend cannot be attributed exclusively to topology. Hence, the chemical contribution seems to be of equal importance, as the studies by Wilden et al. rather suggested for sulfur itself to manipulate the chemistry of Ti-Ni-S liquids, by reducing the melt dynamics, presumably caused by the formation of covalent interactions [33]. The melt viscosity was more than doubled in the ternary Ti-Ni-S system in direct comparison to binary Ti-Ni. The correlation between the maximum GFA and the (Ti,Zr)/(Cu,Ni) to S content appears to be decisive and is worth noting, although further work is necessary to systematically validate this correlation. A more general explanation for the improved GFA in the system studied can be attributed to the predominant formation of the I-phase as primary precipitating phase upon heating from the glassy state (Fig. SI1), suggesting an ISRO in the liquid as reported in many alloy systems [53,70–72]. An ISRO likely

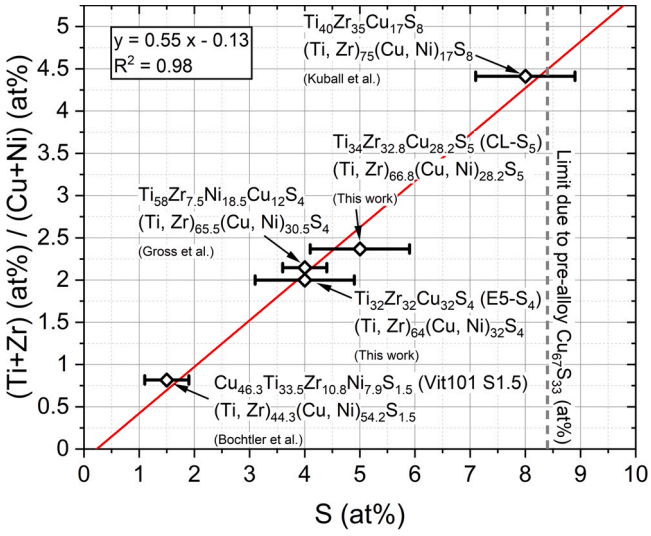

Fig. 6. (Ti+Zr)/(Cu+Ni) ratio as a function of the S content for different BMGs in the (Ti,Zr)-(Cu,Ni)-S system. The compositions $Ti_{40}Zr_{35}Cu_{17}S_8$, $Ti_{58}Zr_{7.5}Ni_{18.5}Cu_{12}S_4$ and $Cu_{46.3}Ti_{33.5}Zr_{10.8}Ni_{7.9}S_{1.5}$ originate from Ref. [20], [19] and [68], respectively. The error bars result from the screening increments of S content performed for each alloy system. When the S content was screened in 1 at% increments, the optimum S content is narrowed down to about ± 0.9 at%. By screening in steps of 0.5 at%, the GFA maximum was determined with an accuracy of about ± 0.4 at% around the ideal S content. The solid red line represents a linear fit with a R^2 of 0.98.

contributes to reduced atomic mobility coupled with an increase in melt viscosity [73–75]. A similar slowdown in melt dynamics is also expected here, resulting in an improved GFA.

The composition $Ti_{40}Zr_{35}Cu_{17}S_8$ is reported to exhibit a higher total strain of ~4.3% compared to the specimen of same composition tested in this work with only 3.2% (Table 2) [20]. However, the higher reported strain is not surprising, since the measured sample size in this work was significantly larger and the formation of shear bands strongly depends on specimen size [76,77]. In addition, smaller specimens possess a higher fictive temperature due to the faster cooling rate and therefore a higher degree of free volume, promoting multiple shear band formation [78–80]. Jiang et al. reported a similar dependence of total strain on specimen dimensions [64]. For this reason, all beams studied in this work have the same dimensions allowing a robust comparability among them. In several other S containing systems, increasing S content led to an embrittlement of the matrix as in

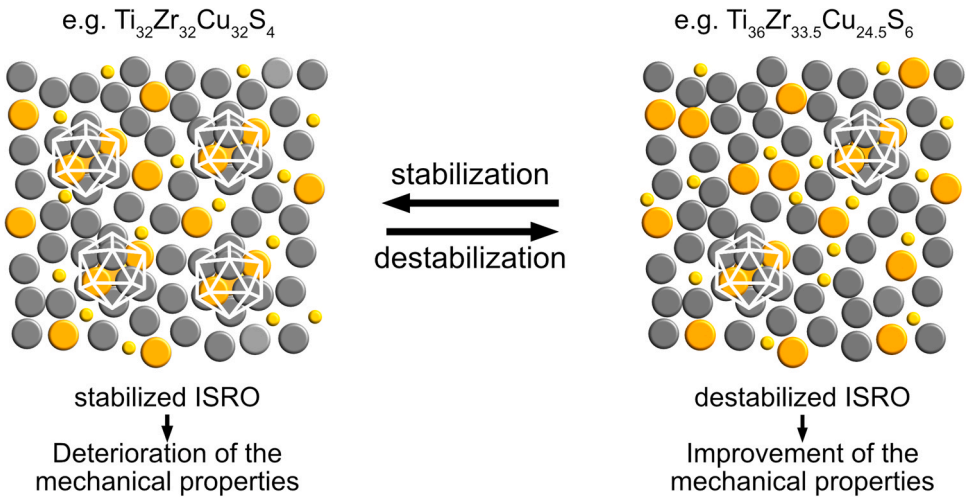

Fig. 7. Schematic visualization of a stabilized and destabilized ISRO. The left and right side depicts exemplarily the structure of an alloy with an increased and decreased number of icosahedral motifs, respectively.

the case of Cu-Zr-Al-S and Pd-Ni-S alloys [42,64]. For Ti-based BMGs, this seems to be different, as the mechanical properties strongly depend on the fractions of the residual constituents by how they stabilize or destabilize the ISRO. Obviously, the mechanical properties are directly related to the intrinsic amorphous structure, i.e. the short-range and medium-range order as well as free volume in the glass (see Fig. SI4) [38,56]. Fig. 7 schematically depicts how a stabilization/destabilization of the ISRO could be understood. The schematic on the left side exemplifies the structure of the composition E5-S_4 with the highest GFA derived from the ternary Ti-Zr-Cu eutectic. A stabilized ISRO is indicated by an increased number of icosahedral motifs, which is also expected for the studied alloys containing Ni and Al. The former is a well-known element stabilizing an icosahedral structure in Ti-based systems [40]. However, small additions of Al also tend to increase the stability of icosahedral structures by forming stable Al-centered icosahedra instead of Cu-centered icosahedra, dominating in Cu-Zr based alloys [81]. A more destabilized ISRO is coupled with a reduced number of icosahedral motifs as outlined on the right side of Fig. 7. The idea is that targeted alloy development strategies (as done for the „connection line“ shown in Fig. 2) lead to reduced number of closed-packed icosahedral motifs, resulting in "less densely packed" regions with higher degree of free volume. This promotes the formation of shear transformation zones and ultimately shear bands [78,82], culminating in a transition from brittle to ductile as observed in Fig. 5a from E5-S_4 to CL-S_6. The present work suggests that the primary formation of crystalline phases during cooling provides information about the ISRO structure in the liquid state and thus also in the glassy state if nucleation has been suppressed. Once quasi-crystalline or crystalline phases are formed that contain icosahedral units (e.g. I-phase and Laves phase observed in all alloy series, see Fig. 1, Fig. 3 and Fig. 4), it is likely that the ISRO is stabilized, resulting in low thermal stability without a distinct SCLR [63]. Considering that the maximum state of an ISRO is the I-phase and that the Laves phase also contains a high proportion of icosahedral clusters, it is not surprising that Ti-based BMGs with a stabilized ISRO behave macroscopically brittle, analogous to the complex crystalline phases [38,63,83–85]. In contrast, the compositions that primarily form quasi-binary $(Ti,Zr)_2Cu$ intermetallic with a tetragonal structure instead of a complex structure exhibit a correspondingly less pronounced, destabilized ISRO, which ultimately translates into improved thermal stability and mechanical properties (e.g. CL-S_6, CL-S_7 and CL-S_8 in Fig. 3 and Fig. 5a). Thus, the formation of simple phases in Ti-based BMGs appear to indicate a structure that favors higher ductility in the amorphous state. For instance, Wang et al. found Ti-based BMGs with high ductility in compression by intentionally choosing a eutectic system containing a ductile B2 phase instead of a complex phase with a Frank-Kasper structure [38]. However, a simple crystalline structure is usually accompanied by reduced GFA due to the higher cooling rates required to suppress crystallization of this simple phase. Here, the alloys with the highest GFA $Ti_{34}Zr_{32.8}Cu_{28.2}S_5$ and $(Ti_{36}Zr_{33.5}Cu_{24.5}S_6)_{97}Al_3$ always precipitate the complex Laves phase (see Fig. 3b, Fig. 4d), coupled by poor mechanical properties. This brittle behavior is altered if the primary crystalline phase changes by further alloy optimization. Our systematic study demonstrates that a judicious manipulation of the short-range order through alloying strategies allows the synthesis of compositions with superior mechanical properties coupled with improved GFA by analyzing the primary crystals as well as thermal stability. Ideally, a single XRD/DSC measurement is sufficient to judge whether or not alloy development is proceeding towards promising mechanical properties as the primary crystalline phases as well as the thermal stability mirrors the prevailing glassy structure. In other words, if the I- or Laves phase are primarily formed, which is related to a low thermal stability, there is no need for an extensive investigation of the mechanical properties, since a predominantly brittle fracture behavior is to be expected. However, if the XRD measurement indicate a simpler crystalline phase, such as $(Ti,Zr)_2Cu$, it is worth to investigate the mechanical performance, as good properties with a certain ductility are expected.

To summarize and graphically elucidate our findings, schematic time-temperature-transformation (TTT) diagrams for the different alloying strategies shown in Fig. 8a to c were constructed from the XRD crystallization data at different thicknesses as well as the knowledge of the first crystallizing phase upon heating (Fig. SI2). Since no TTT diagrams were measured experimentally in this work, the graphs are simply a proposed schematic visualization of the individual alloying strategies and their influence on the crystallization behavior. The effect of S on the position of the crystallization curves of the Laves phase and $(Ti,Zr)_2Cu$ phase is illustrated in Fig. 8a (solid blue and orange lines). The two lines are drawn right next to each other, as both phases are detected in the XRD patterns. An increasing S content pushes both crystallization “noses” to longer times due to the higher GFA and lower critical cooling rate required for glass formation, which is reflected in the maximum d_c of 4 mm at an optimum S content of 4 at%. Even higher S contents in turn lead to a reduction in GFA to 500 µm for S_{10} and thus to shorter "nose" times, indicated by dashed lines (Fig. 1). The DSC measurements revealed a continuous stabilization of the SCL from initially no visible T_g due to the formation of the I-phase to a broad SCLR of 72 K

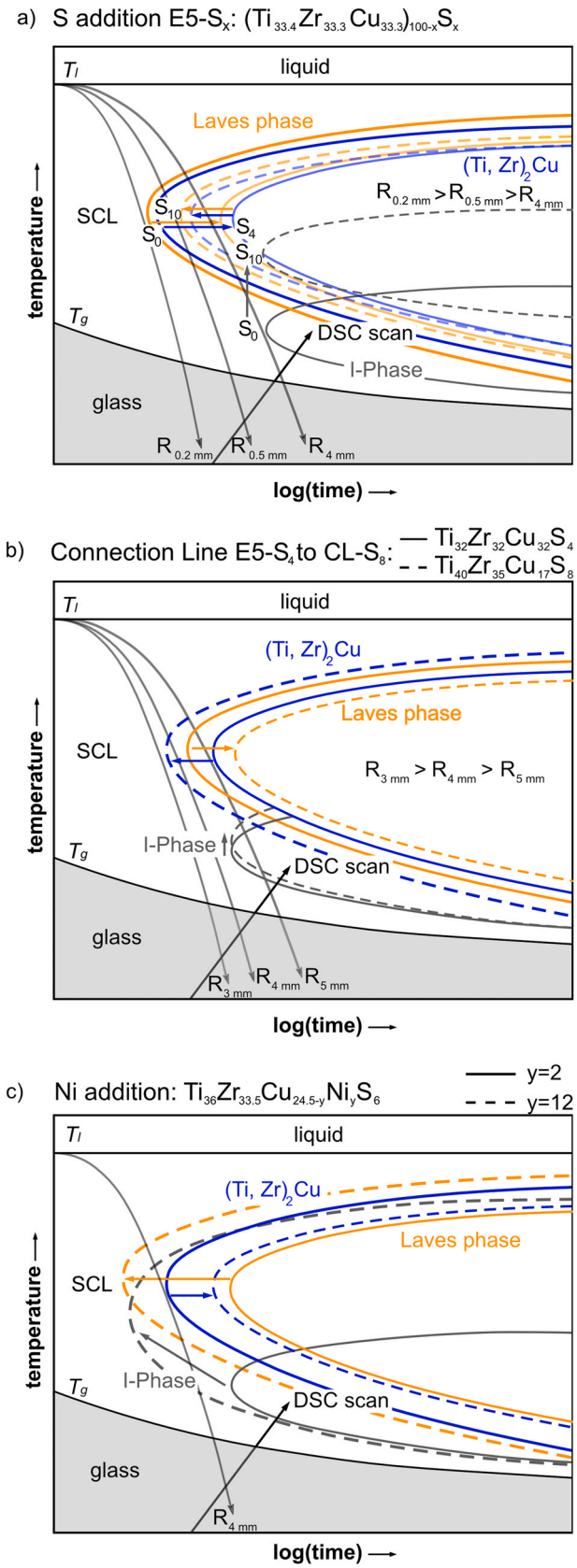

Fig. 8. The schematic TTT diagrams illustrate (a) the influence of increasing S content on the crystallization curves, (b) their change along the "connecting line" from $Ti_{32}Zr_{32}Cu_{32}S_4$ (E5-S_4) to $Ti_{40}Zr_{35}Cu_{17}S_8$ (CL-S_8), and (c) the influence of Ni addition. The solid lines represent the initial state and the dashed lines the final state of the respective alloying strategy. The arrows indicate the movement of the crystallization curves of each phase, while orange lines represent the Laves phase, blue lines the (Ti, Zr)$_2$Cu intermetallic and gray lines the icosahedral phase.

at S_{10} due to the complete destabilization of this phase. In the latter, the I-phase no longer crystallizes, but the Laves phase, which is indicated by a shift of the TTT diagram of the I-phase from the grey continuous to the grey dashed line. The plotted cooling rates $R_{0.2\,mm}$, $R_{4\,mm}$ and $R_{0.5\,mm}$ to bypass the tip of the respective crystallization curve indicate the critical cooling rate for E5-S_0, E5-S_4 and E5-S_{10}, respectively, which can be estimated from the critical casting thickness d_c according to Lin et al. (R=10/d_c^2, d_c in cm) [86]. Fig. 8b depicts the change in crystallization across the "connection line". The cooling curve $R_{5\,mm}$ crosses either the Laves or the (Ti,Zr)$_2$Cu curve at any point, as no fully amorphous 5 mm XRD patterns were obtained (see Fig. 3). As (Ti,Zr)$_2$Cu becomes the primary crystalline phase on the way to $Ti_{40}Zr_{35}Cu_{17}S_8$, there is consequently an interchange with the Laves phase. This point was observed at $Ti_{34}Zr_{32.8}Cu_{28.2}S_5$, where both phases were coexisting. Overall, the (Ti,Zr)$_2$Cu crystal curve shifts to shorter times as the $Ti_{40}Zr_{35}Cu_{17}S_8$ composition contains a reduced GFA compared to the initial composition $Ti_{32}Zr_{32}Cu_{32}S_4$. Regarding the I-phase, a similar trend to the first case of continuous stabilization of the SCL can be observed, but not to a similar extent, as the I-phase stays the primary precipitating phase upon heating. The Al-series behaves basically in the same manner, but in the opposite direction, as Al addition leads to a change from the (Ti,Zr)$_2$Cu phase to the Laves phase and reduced thermal stability. With increasing Ni content on the other hand (Fig. 8c), the TTT curve for the I-phase is shifted to the left and dominates the crystallization process, which increases the critical cooling rate required for glass formation and reduces the thermal stability against crystallization. Both are likely attributable to a low interfacial energy with respect to the supercooled liquid or glass, resulting in a low nucleation barrier as discussed above [41,54–57]. Therefore, the removal of Ni to precipitate a crystalline phase instead of a quasi-crystalline phase is desirable in terms of GFA, thermal stability and mechanical properties. This also accommodates its use as a potential biocompatible light weight material.

5. Summary and conclusion

The influence of S on the GFA, thermal stability and mechanical properties of the eutectic composition $Ti_{33.4}Zr_{33.3}Cu_{33.3}$ was investigated. Minor additions of sulfur with an ideal content of 4 at% S significantly improved the GFA by increasing the critical casting diameter from 200 µm to 4 mm. Likewise improved was the thermal stability by destabilizing the icosahedral phase upon heating, however, the optimum in glass formation does not coincide with the largest SCLR. A putative correlation was established between the ratio of (Ti,Zr) to (Cu,Ni) and the ideal S content required to achieve the highest GFA. Due to the brittle nature of the novel composition $Ti_{32}Zr_{32}Cu_{32}S_4$ with the highest critical casting thickness, targeted alloying strategies were employed, resulting in an optimized alloy $Ti_{36}Zr_{33.5}Cu_{24.5}S_6$ with the same GFA of 4 mm but a ductile fracture behavior in bending. Furthermore, a correlation between the primary crystallizing phase, the thermal stability and the mechanical properties in a S-bearing Ti-based bulk glass forming system was found. Alloy compositions which form primarily the I- or Laves-phase are more prone to a brittle fracture, whereas glasses that primary crystallize as (Ti,Zr)$_2$Cu from the high temperature liquid tend to exhibit a plastic regime in 3PBB experiments. This observation is presumably connected to the atomic short-range order in the liquid state, being less dominated by ISRO for liquids primary crystallizing as (Ti,Zr)$_2$Cu. Moreover, a destabilized ISRO is mirrored by improved thermal stability, as a result of the destabilization of the I-phase upon heating. Our study shows that the detection of the primary precipitating phase and thermal stability can have high informative value about the mechanical performance of bulk metallic glasses and should be considered as important indicator for the development of for engineering-oriented glass forming alloys.

CRediT authorship contribution statement

Lucas M. Ruschel: Writing – original draft, Project administration, Methodology, Investigation, Formal analysis, Data curation, Conceptualization. **Bastian Adam:** Writing – review & editing, Project administration, Investigation, Formal analysis. **Oliver Gross:** Writing – review & editing, Supervision, Formal analysis, Visualization. **Nico Neuber:** Writing – review & editing, Formal analysis, Data curation. **Maximilian Frey:** Writing – review & editing, Formal analysis, Data curation. **Hans-Jürgen Wachter:** Writing – review & editing, Supervision, Project administration, Resources. **Ralf Busch:** Writing – review & editing, Supervision, Project administration, Funding acquisition.

Data Availability

Data will be made available on request.

Declaration of Competing Interest

The authors declare that they have no known competing financial interests or personal relationships that could have appeared to influence the work reported in this paper.

Acknowledgements

The authors would like to thank F. Aubertin, I. Gallino, B. Bochtler and A. Kuball for many fruitful discussions. This research was conducted and funded in collaboration with Heraeus AMLOY Technologies GmbH. They also supplied the raw elements for the production of the alloys. This research was also partially supported by the German Research Foundation (DFG) through Grant No. BU 2276/10-1 and No. BU 2276/11-1. Moreover, instrumentation and technical assistance for this work were provided by the Service Center X-ray Diffraction, with financial support from Saarland University and German Science Foundation (project number INST 256/349-1). The authors thank Dr. Oliver Janka and Tobias Straub for the support in collection of the X-ray diffraction data presented in this paper.

Appendix A. Supporting information

Supplementary data associated with this article can be found in the online version at doi:10.1016/j.jallcom.2023.170614.

References

[1] W. Klement, R. Willens, P. Duwez, Non-crystalline structure in solidified gold–silicon alloys, Nature 187 (1960) 869–870, https://doi.org/10.1038/187869b0
[2] A.L. Greer, E. Ma, Bulk metallic glasses: at the cutting edge of metals research, MRS Bull. 32 (2007) 611–619, https://doi.org/10.1557/mrs2007.121
[3] T. Zhang, A. Inoue, T. Masumoto, Amorphous Zr-Al-TM (TM=Co, Ni, Cu) alloys with significant supercooled liquid region of over 100 K, Mater. Trans. JIM 32 (1991) 1005–1010, https://doi.org/10.2320/matertrans1989.32.1005
[4] S.L. Zhu, X.M. Wang, F.X. Qin, A. Inoue, A new Ti-based bulk glassy alloy with potential for biomedical application, Mater. Sci. Eng. A 459 (2007) 233–237, https://doi.org/10.1016/j.msea.2007.01.044
[5] N. Nishiyama, K. Takenaka, H. Miura, N. Saidoh, Y. Zeng, A. Inoue, The world's biggest glassy alloy ever made, Intermetallics 30 (2012) 19–24, https://doi.org/10.1016/j.intermet.2012.03.020
[6] T. Zhang, A. Inoue, Bulk glassy alloys with low liquidus temperature in Pt-Cu-P system, Mater. Trans. 44 (2003) 1143–1146, https://doi.org/10.2320/matertrans.44.1143
[7] J. Schroers, W.L. Johnson, Ductile bulk metallic glass, Phys. Rev. Lett. 93 (2004) 255506, https://doi.org/10.1103/PhysRevLett.93.255506
[8] O. Gross, M. Eisenbart, L.-Y. Schmitt, N. Neuber, L. Ciftci, U.E. Klotz, R. Busch, I. Gallino, Development of novel 18-karat, premium-white gold bulk metallic glasses with improved tarnishing resistance, Mater. Des. 140 (2018) 495–504, https://doi.org/10.1016/j.matdes.2017.12.007
[9] M. Frey, R. Busch, W. Possart, I. Gallino, On the thermodynamics, kinetics, and sub-Tg relaxations of Mg-based bulk metallic glasses, Acta Mater. 155 (2018) 117–127, https://doi.org/10.1016/j.actamat.2018.05.063
[10] A. Inoue, B.L. Shen, C.T. Chang, Super-high strength of over 4000 MPa for Fe-based bulk glassy alloys in [(Fe1−xCox)0.75B0.2Si0.05]96Nb4 system, Acta Mater. 52 (2004) 4093–4099, https://doi.org/10.1016/j.actamat.2004.05.022
[11] L. Xia, W.H. Li, S.S. Fang, B.C. Wei, Y.D. Dong, Binary Ni–Nb bulk metallic glasses, J. Appl. Phys. 99 (2006) 026103, https://doi.org/10.1063/1.2158130
[12] L.M. Ruschel, O. Gross, B. Bochtler, B. Li, B. Adam, N. Neuber, M. Frey, S. Jakovlev, F. Yang, H. Jiang, B. Gludovatz, J.J. Kruzic, R. Busch, Ni-Nb-P-based bulk glass-forming alloys: Superior material properties combined in one alloy family, Acta Mater 253 (2023) 118968, https://doi.org/10.1016/j.actamat.2023.118968
[13] Y.C. Kim, W.T. Kim, D.H. Kim, A development of Ti-based bulk metallic glass, Mater. Sci. Eng. A 375–377 (2004) 127–135, https://doi.org/10.1016/j.msea.2003.10.115
[14] P. Gong, X. Wang, Y. Shao, N. Chen, X. Liu, K.F. Yao, A Ti–Zr–Be–Fe–Cu bulk metallic glass with superior glass-forming ability and high specific strength, Intermetallics 43 (2013) 177–181, https://doi.org/10.1016/j.intermet.2013.08.003
[15] S. Lin, D. Liu, Z. Zhu, D. Li, H. Fu, Y. Zhuang, H. Zhang, H. Li, A. Wang, H. Zhang, New Ti-based bulk metallic glasses with exceptional glass forming ability, J. Non Cryst. Solids 502 (2018) 71–75, https://doi.org/10.1016/j.jnoncrysol.2018.06.038
[16] S.L. Zhu, X.M. Wang, A. Inoue, Glass-forming ability and mechanical properties of Ti-based bulk glassy alloys with large diameters of up to 1 cm, Intermetallics 16 (2008) 1031–1035, https://doi.org/10.1016/j.intermet.2008.05.006
[17] J.-J. Oak, D.V. Louzguine-Luzgin, A. Inoue, Investigation of glass-forming ability, deformation and corrosion behavior of Ni-free Ti-based BMG alloys designed for application as dental implants, Mater. Sci. Eng. C. 29 (2009) 322–327, https://doi.org/10.1016/j.msec.2008.07.009
[18] J.C. Schuster, G. Cacciamani, The Cu-Ni-Ti (Copper-Nickel-Titanium) system, J. Phase Equilibria. 23 (2002) 541–547, https://doi.org/10.1361/105497102770331299
[19] O. Gross, L. Ruschel, A. Kuball, B. Bochtler, B. Adam, R. Busch, Bulk metallic glass formation in the (Ti,Zr)-(Ni,Cu)-S system, J. Phys. Condens. Matter 84 (2020) 4029–4031, https://doi.org/10.1088/1361-648X/ab7c15
[20] A. Kuball, O. Gross, B. Bochtler, B. Adam, L. Ruschel, M. Zamanzade, R. Busch, Development and characterization of titanium-based bulk metallic glasses, J. Alloy. Compd. 790 (2019) 337–346, https://doi.org/10.1016/j.jallcom.2019.03.001
[21] Y. Ingenbleek, H. Kimura, Nutritional essentiality of sulfur in health and disease, Nutr. Rev. 71 (2013) 413–432, https://doi.org/10.1111/nure.12050
[22] M. Geetha, A.K. Singh, R. Asokamani, A.K. Gogia, Ti based biomaterials, the ultimate choice for orthopaedic implants – A review, Prog. Mater. Sci. 54 (2009) 397–425, https://doi.org/10.1016/j.pmatsci.2008.06.004
[23] H.F. Li, Y.F. Zheng, Recent advances in bulk metallic glasses for biomedical applications, Acta Biomater. 36 (2016) 1–20, https://doi.org/10.1016/j.actbio.2016.03.047
[24] S. Pang, Y. Liu, H. Li, L. Sun, Y. Li, T. Zhang, New Ti-based Ti–Cu–Zr–Fe–Sn–Si–Ag bulk metallic glass for biomedical applications, J. Alloy. Compd. 625 (2015) 323–327, https://doi.org/10.1016/j.jallcom.2014.07.021
[25] Y. Liu, G. Wang, H. Li, S. Pang, K. Chen, T. Zhang, Ti-Cu-Zr-Fe-Sn-Si-Sc bulk metallic glasses with good mechanical properties for biomedical applications, J. Alloy. Compd. 679 (2016) 341–349, https://doi.org/10.1016/j.jallcom.2016.03.224
[26] R. Arroyave, T.W. Eagar, L. Kaufman, Thermodynamic assessment of the Cu–Ti–Zr system, J. Alloy. Compd. 351 (2003) 158–170, https://doi.org/10.1016/S0925-8388(02)01035-6
[27] A. Inoue, 1997. Stabilization of Supercooled Liquid and Opening-up of Bulk Glassy Alloys., Proc. Japan Acad. Ser. B. 73 (1997) 19–24. ⟨https://doi.org/10.2183/pjab.73.19⟩.
[28] V.V. Molokanov, V.N. Chebotnikov, Glass forming ability, structure and properties of Ti and Zr-Intermetallic compound based alloys, Key Eng. Mater. 40–41 (1991) 319–332, https://doi.org/10.4028/www.scientific.net/KEM.40-41.319
[29] W.H. Wang, Roles of minor additions in formation and properties of bulk metallic glasses, Prog. Mater. Sci. 52 (2007) 540–596, https://doi.org/10.1016/j.pmatsci.2006.07.003
[30] Z.P. Lu, C.T. Liu, Role of minor alloying additions in formation of bulk metallic glasses: A Review, J. Mater. Sci. 39 (2004) 3965–3974, https://doi.org/10.1023/B:JMSC.0000031478.73621.64
[31] N. Nollmann, I. Binkowski, V. Schmidt, H.R.?? sner, G. Wilde, H. Rösner, G. Wilde, Impact of micro-alloying on the plasticity of Pd-based bulk metallic glasses, Scr. Mater. 111 (2016) 119–122, https://doi.org/10.1016/j.scriptamat.2015.08.030
[32] A. Kuball, O. Gross, B. Bochtler, R. Busch, Sulfur-bearing metallic glasses: a new family of bulk glass-forming alloys, Scr. Mater. 146 (2018) 73–76, https://doi.org/10.1016/j.scriptamat.2017.11.011
[33] J. Wilden, F. Yang, D. Holland-Moritz, S. Szabó, W. Lohstroh, B. Bochtler, R. Busch, A. Meyer, Impact of Sulfur on the melt dynamics of glass forming Ti 75 Ni 25− x S x, Appl. Phys. Lett. 117 (2020) 013702, https://doi.org/10.1063/5.0012409
[34] B. Lu, Y. Li, J. Xu, Optimal glass-forming composition and its correlation with eutectic reaction in the Ti–Ni–Al ternary system, J. Alloy. Compd. 467 (2009) 261–267, https://doi.org/10.1016/j.jallcom.2007.12.050
[35] B.-C. Lu, Y.-L. Wang, J. Xu, Revisiting the glass-forming ability of Ti–Ni–Si ternary alloys, J. Alloy. Compd. 475 (2009) 157–164, https://doi.org/10.1016/j.jallcom.2008.07.055
[36] L. Wang, L. Ma, C. Ma, A. Inoue, Formations of amorphous and quasicrystal phases in Ti–Zr–Ni–Cu alloys, J. Alloy. Compd. 361 (2003) 234–240, https://doi.org/10.1016/S0925-8388(03)00430-4
[37] C. Ma, S. Ishihara, H. Soejima, N. Nishiyama, A. Inoue, Formation of new Ti-based metallic glassy alloys, Mater. Trans. 45 (2004) 1802–1806, https://doi.org/10.2320/matertrans.45.1802
[38] Y.-L. Wang, J. Xu, Ti (Zr)-Cu-Ni bulk metallic glasses with optimal glass-forming ability and their compressive properties, Metall. Mater. Trans. A. 39 (2008) 2990–2997, https://doi.org/10.1007/s11661-008-9647-6

[39] K. Kelton, A. Gangopadhyay, G. Lee, L. Hannet, R.W. Hyers, S. Krishnan, M.B. Robinson, J. Rogers, T.J. Rathz, X-ray and electrostatic levitation undercooling studies in Ti–Zr–Ni quasicrystal forming alloys, J. Non Cryst. Solids 312–314 (2002) 305–308, https://doi.org/10.1016/S0022-3093(02)01691-5
[40] G.W. Lee, A.K. Gangopadhyay, R.W. Hyers, T.J. Rathz, J.R. Rogers, D.S. Robinson, A.I. Goldman, K.F. Kelton, Local structure of equilibrium and supercooled Ti-Zr-Ni liquids, Phys. Rev. B. 77 (2008) 184102, https://doi.org/10.1103/PhysRevB.77.184102
[41] G.W. Lee, A.K. Gangopadhyay, T.K. Croat, T.J. Rathz, R.W. Hyers, J.R. Rogers, K.F. Kelton, Link between liquid structure and the nucleation barrier for icosahedral quasicrystal, polytetrahedral, and simple crystalline phases in Ti-Zr-Ni alloys: Verification of Frank's hypothesis, Phys. Rev. B. 72 (2005) 174107, https://doi.org/10.1103/PhysRevB.72.174107
[42] A. Kuball, B. Bochtler, O. Gross, V. Pacheco, M. Stolpe, S. Hechler, R. Busch, On the bulk glass formation in the ternary Pd-Ni-S system, Acta Mater. 158 (2018) 13–22, https://doi.org/10.1016/j.actamat.2018.07.039
[43] K.J. Laws, D.B. Miracle, M. Ferry, A predictive structural model for bulk metallic glasses, Nat. Commun. 6 (2015) 8123, https://doi.org/10.1038/ncomms9123
[44] A. Takeuchi, A. Inoue, Classification of bulk metallic glasses by atomic size difference, heat of mixing and period of constituent elements and its application to characterization of the main alloying element, Mater. Trans. 46 (2005) 2817–2829, https://doi.org/10.2320/matertrans.46.2817
[45] Y.C. Kim, J.M. Park, J.K. Lee, D.H. Bae, W.T. Kim, D.H. Kim, Amorphous and icosahedral phases in Ti–Zr–Cu–Ni–Be alloys, Mater. Sci. Eng. A 375–377 (2004) 749–753, https://doi.org/10.1016/j.msea.2003.10.116
[46] J.N. Mei, J.S. Li, H.C. Kou, J.L. Soubeyroux, H.Z. Fu, L. Zhou, Formation of Ti–Zr–Ni–Cu–Be–Nb bulk metallic glasses, J. Alloy. Compd. 467 (2009) 235–240, https://doi.org/10.1016/j.jallcom.2007.12.066
[47] J.M. Park, H.J. Chang, K.H. Han, W.T. Kim, D.H. Kim, Enhancement of plasticity in Ti-rich Ti–Zr–Be–Cu–Ni bulk metallic glasses, Scr. Mater. 53 (2005) 1–6, https://doi.org/10.1016/j.scriptamat.2005.03.024
[48] L. Wang, A. Inoue, Icosahedral and amorphous phases in Melt-Spun Ti-Zr-Ni-Cu alloys, Mater. Trans. 42 (2001) 2637–2640, https://doi.org/10.2320/matertrans.42.2637
[49] M.E. Stiehler, N.T. Panagiotopoulos, D.S. Keeble, Y.P. Ivanov, M. Menelaou, M.R. Jolly, A. Lindsay Greer, K. Georgarakis, The effect of Ni or Co additions on the structure of Zr60Cu30Al10 bulk metallic glass revealed by high-energy synchrotron radiation, Mater. Today Commun. 31 (2022) 103531, https://doi.org/10.1016/j.mtcomm.2022.103531
[50] J. Saida, C. Li, M. Matsushita, A. Inoue, Investigation of the stability of glassy state in the Zr- and Hf-based glassy alloys correlated with their transformation behavior, J. Mater. Res. 16 (2001) 3389–3401, https://doi.org/10.1557/JMR.2001.0467
[51] J.N. Mei, J.S. Li, H.C. Kou, H.Z. Fu, L. Zhou, Effects of Nb on the formation of icosahedral quasicrystalline phase in Ti-rich Ti–Zr–Ni–Cu–Be glassy forming alloys, J. Non Cryst. Solids 354 (2008) 3332–3335, https://doi.org/10.1016/j.jnoncrysol.2008.02.001
[52] X. Zhou, H. Kou, J. Wang, J. Li, L. Zhou, Crystallization and compressive behaviors of Ti40Zr25Ni8Cu9Be18 BMG cast from different liquid states, Intermetallics 28 (2012) 45–50, https://doi.org/10.1016/j.intermet.2012.03.061
[53] J. Saida, M. Matsushita, A. Inoue, Formation of the icosahedral quasicrystalline phase in Zr 70 Pd 30 binary glassy alloy, Philos. Mag. Lett. 81 (2001) 39–44, https://doi.org/10.1080/09500830010007476
[54] Y.C. Kim, J.H. Na, J.M. Park, D.H. Kim, J.K. Lee, W.T. Kim, Role of nanometer-scale quasicrystals in improving the mechanical behavior of Ti-based bulk metallic glasses, Appl. Phys. Lett. 83 (2003) 3093–3095, https://doi.org/10.1063/1.1616198
[55] F. Spaepen, A structural model for the solid-liquid interface in monatomic systems, Scr. Metall. 9 ((1975) xvii, https://doi.org/10.1016/0036-9748(75)90195-7
[56] Z.W. Zhu, L. Gu, G.Q. Xie, W. Zhang, A. Inoue, H.F. Zhang, Z.Q. Hu, Relation between icosahedral short-range ordering and plastic deformation in Zr–Nb–Cu–Ni–Al bulk metallic glasses, Acta Mater. 59 (2011) 2814–2822, https://doi.org/10.1016/j.actamat.2011.01.020
[57] F. Guo, H.-J. Wang, S.J. Poon, G.J. Shiflet, Ductile titanium-based glassy alloy ingots, Appl. Phys. Lett. 86 (2005) 091907, https://doi.org/10.1063/1.1872214
[58] O. Gross, S.S. Riegler, M. Stolpe, B. Bochtler, A. Kuball, S. Hechler, R. Busch, I. Gallino, On the high glass-forming ability of Pt-Cu-Ni/Co-P-based liquids, Acta Mater. 141 (2017) 109–119, https://doi.org/10.1016/j.actamat.2017.09.013
[59] S.K. Das, J.H. Perepezko, R.I. Wu, G. Wilde, Undercooling and glass formation in Al-based alloys, Mater. Sci. Eng. A. 304–306 (2001) 159–165, https://doi.org/10.1016/S0921-5093(00)01483-0
[60] A. Kuball, M. Stolpe, R. Busch, Crystallization behavior of the Al86Ni8Y6 metallic glass forming alloy upon rapid cooling, J. Alloy. Compd. 737 (2018) 398–404, https://doi.org/10.1016/j.jallcom.2017.12.044
[61] J.P. Liao, B.J. Yang, Y. Zhang, W.Y. Lu, X.J. Gu, J.Q. Wang, Evaluation of glass formation and critical casting diameter in Al-based metallic glasses, Mater. Des. 88 (2015) 222–226, https://doi.org/10.1016/j.matdes.2015.08.138
[62] K. Sugiyama, K. Yasuda, Y. Horikawa, T. Ohsuna, K. Hiraga, Crystal structure of μ7-MgZnSm, J. Alloy. Compd. 285 (1999) 172–178, https://doi.org/10.1016/S0925-8388(98)01048-2
[63] R.W. Cahn, P. Haasen, Physical Metallurgy, Fourth ed., Elsevier Science B.V., Amsterdam, The Netherlands, 1996.
[64] H. Jiang, J. Hu, N. Neuber, B. Bochtler, B. Adam, S.S. Riegler, M. Frey, L. Ruschel, W. Lu, A. Feng, R. Busch, J. Shen, Effect of sulfur on the glass-forming ability, phase transformation, and thermal stability of Cu-Zr-Al bulk metallic glass, Acta Mater. 212 (2021) 116923, https://doi.org/10.1016/j.actamat.2021.116923
[65] J.L. Murray, The Ti–Zr (Titanium-Zirconium) system, Bull. Alloy Phase Diagr. 2 (1981) 197–201, https://doi.org/10.1007/BF02881478
[66] J. Miettinen, Thermodynamic description of the Cu-Al-Ni system at the Cu-Ni side, Calphad Comput. Coupling Phase Diagr. Thermochem. 29 (2005) 40–48, https://doi.org/10.1016/j.calphad.2005.02.002
[67] S. Pauly, J. Das, J. Bednarcik, N. Mattern, K. Kim, D. Kim, J. Eckert, Deformation-induced martensitic transformation in Cu–Zr–(Al,Ti) bulk metallic glass composites, Scr. Mater. 60 (2009) 431–434, https://doi.org/10.1016/j.scriptamat.2008.11.015
[68] B. Bochtler, 2019. Thermophysical and Structural Investigations of a CuTi- and a Zr-based Bulk Metallic Glass, the Influence of Minor Additions, and the Relation to Thermoplastic Forming, Saarland University, 2019.
[69] Z. Lu, C. Liu, Y. Dong, Effects of atomic bonding nature and size mismatch on thermal stability and glass-forming ability of bulk metallic glasses, J. Non Cryst. Solids 341 (2004) 93–100, https://doi.org/10.1016/j.jnoncrysol.2004.04.024
[70] K.F. Kelton, G.W. Lee, A.K. Gangopadhyay, R.W. Hyers, T.J. Rathz, J.R. Rogers, M.B. Robinson, D.S. Robinson, First X-Ray scattering studies on electrostatically levitated metallic liquids: demonstrated influence of local icosahedral order on the nucleation barrier, Phys. Rev. Lett. 90 (2003) 195504, https://doi.org/10.1103/PhysRevLett.90.195504
[71] Y. Shen, S.J. Poon, G.J. Shiflet, Crystallization of icosahedral phase from glassy Pd-U-Si alloys, Phys. Rev. B. 34 (1986) 3516–3519, https://doi.org/10.1103/PhysRevB.34.3516
[72] L.Q. Xing, T.C. Hufnagel, J. Eckert, W. Löser, L. Schultz, Relation between short-range order and crystallization behavior in Zr-based amorphous alloys, Appl. Phys. Lett. 77 (2000) 1970–1972, https://doi.org/10.1063/1.1313255
[73] S. Mukherjee, J. Schroers, W.L. Johnson, W.-K. Rhim, Influence of kinetic and thermodynamic factors on the glass-forming ability of zirconium-based bulk amorphous alloys, Phys. Rev. Lett. 94 (2005) 245501, https://doi.org/10.1103/PhysRevLett.94.245501
[74] H. Tanaka, Roles of local icosahedral chemical ordering in glass and quasicrystal formation in metallic glass formers, J. Phys. Condens. Matter 15 (2003) L491–L498, https://doi.org/10.1088/0953-8984/15/31/102
[75] S. Sachdev, D.R. Nelson, Theory of the structure factor of metallic glasses, Phys. Rev. Lett. 53 (1984) 1947–1950, https://doi.org/10.1103/PhysRevLett.53.1947
[76] G. Kumar, A. Desai, J. Schroers, Bulk metallic glass: the smaller the better, Adv. Mater. 23 (2011) 461–476, https://doi.org/10.1002/adma.201002148
[77] R.D. Conner, W.L. Johnson, N.E. Paton, W.D. Nix, Shear bands and cracking of metallic glass plates in bending, J. Appl. Phys. 94 (2003) 904–911, https://doi.org/10.1063/1.1582555
[78] C. Schuh, T. Hufnagel, U. Ramamurty, Mechanical behavior of amorphous alloys, Acta Mater. 55 (2007) 4067–4109, https://doi.org/10.1016/j.actamat.2007.01.052
[79] G. Kumar, P. Neibecker, Y.H. Liu, J. Schroers, Critical fictive temperature for plasticity in metallic glasses, Nat. Commun. 4 (2013), https://doi.org/10.1038/ncomms2546
[80] A. Datye, J. Ketkaew, J. Schroers, U.D. Schwarz, Effect of the fictive temperature on the modulus, hardness, yield strength, dynamic mechanical and creep response of Zr44Ti11Cu10Ni10Be25 metallic glasses, J. Alloy. Compd. 819 (2020) 152979, https://doi.org/10.1016/j.jallcom.2019.152979
[81] W. Lu, Z. Wang, H. Xiang, A. Feng, J. Shen, Exploration of the atomic-level structures of the icosahedral clusters in Cu–Zr–Al ternary metallic glasses via first-principles theory, Mater. Res. Express 9 (2022) 065203, https://doi.org/10.1088/2053-1591/ac7516
[82] A. Argon, Plastic deformation in metallic glasses, Acta Met. 27 (1979) 47–58, https://doi.org/10.1016/0001-6160(79)90055-5
[83] U. Köster, H. Liebertz, W. Liu, Plastic deformation of quasi-crystalline and crystalline phases in Al-Cu-Fe alloys, Mater. Sci. Eng. A. 181–182 (1994) 777–780, https://doi.org/10.1016/0921-5093(94)90737-4
[84] Y. Liu, G. Yuan, W. Ding, C. Lu, Deformation behavior of Mg–Zn–Gd-based alloys reinforced with quasicrystal and Laves phases at elevated temperatures, J. Alloy. Compd. 427 (2007) 160–165, https://doi.org/10.1016/j.jallcom.2006.03.027
[85] Y.C. Kim, J.M. Park, J.K. Lee, W.T. Kim, D.H. Kim, Precipitation of stable Icosahedral phase in Ti-Based amorphous alloys, Mater. Trans. 44 (2003) 1978–1981, https://doi.org/10.2320/matertrans.44.1978
[86] X.H. Lin, W.L. Johnson, Formation of Ti–Zr–Cu–Ni bulk metallic glasses, J. Appl. Phys. 78 (1995) 6514–6519, https://doi.org/10.1063/1.360537